Available online at www.sciencedirect.com
SCIENCE DIRECT
Journal of Organometallic Chemistry 691 (2006) 2987–3002
Journal of Organometallic Chemistry
www.elsevier.com/locate/jorganchem

# Electronic properties of new homobimetallic anthracene-bridged $\eta^5$-cyclopentadienyl derivatives of iridium(I) and of the corresponding cation radicals $[L_2Ir\{C_5H_4CH_2(9,10\text{-anthrylene})CH_2C_5H_4\}IrL_2]^{+\cdot}$

Federica Bertini [a], Lucia Calucci [b], Francesca Cicogna [a], Benedetta Gaddi [a], Giovanni Ingrosso [a,*], Massimo Marcaccio [c], Fabio Marchetti [a], Demis Paolucci [c], Francesco Paolucci [c], Calogero Pinzino [b]

[a] *Dipartimento di Chimica e Chimica Industriale, Università di Pisa, Via Risorgimento 35, 56126 Pisa, Italy*
[b] *Istituto per i Processi Chimico-Fisici del C.N.R., Area della Ricerca di Pisa, Via G. Moruzzi 1, 56124 Pisa, Italy*
[c] *Dipartimento di Chimica 'G. Ciamician', Università di Bologna, Via Selmi 2, 40126 Bologna, Italy*

Received 31 January 2006; received in revised form 3 March 2006; accepted 3 March 2006
Available online 16 March 2006

**Abstract**

The bimetallic complexes $[L_2Ir\{C_5H_4CH_2(9,10\text{-anthrylene})CH_2C_5H_4\}IrL_2]$ (**3**) (L = $\eta^2$-$C_2H_4$) and (**4**) (L = CO) were obtained by reacting the thallium(I) derivative of 9,10-bis(cyclopentadienylmethyl)-anthracene (**1**), i.e. $[Tl\{C_5H_4CH_2(9,10\text{-anthrylene})CH_2C_5H_4\}Tl]$ (**2**), with $[IrCl(\eta^2\text{-}C_2H_4)_4]$ and $[IrCl(C_5H_5N)(CO)_2]$, respectively, and characterized by elemental analysis, MS, $^1$H NMR, UV–Vis (290–490 nm) spectroscopy, and FT-IR. When excited at wavelengths ranging from 333 to 383 nm, **1** results to be fluorescent, while **3** and **4** show the almost complete quenching of the anthrylene fluorescence. The electrochemical behaviour of **3** and **4** has been studied and compared with that of the monometallic complexes, i.e. ($\eta^5$-9-anthrylmethylcyclopentadienyl)-bis($\eta^2$-ethylene)iridium(I) (**5**), whose preparation and X-ray structure are reported here, and the already described ($\eta^5$-9-anthrylmethylcyclopentadienyl)dicarbonyliridium(I) (**6**). The study allows the interpretation of the electrode processes and gives information about the location of the redox sites along with the thermodynamic characterization of the redox processes. On this basis, the intramolecular charge-transfer process between the photo-excited anthrylenic moiety and one cyclopentadienyl$IrL_2$ unit is suggested to be a possible route for the quenching of the anthrylene fluorescence. The oxidation of **3** and **4** by [bis(trifluoroacetoxy)iodo]benzene (PIFA) and thallium(III) trifluoroacetate (TTFA), respectively, produces the radical cations $\mathbf{3}^+$ and $\mathbf{4}^+$, which, on the base of their EPR spectra, are described as average-valence [$Ir^{+1.5}$, $Ir^{+1.5}$] species. DFT calculations of spin density distribution confirm the EPR results and allow a further insight into the structure of such radicals. Differences and analogies lying between the electronic and conformational structure of the bimetallic, $\mathbf{3}^+$ and $\mathbf{4}^+$, and the monometallic, $\mathbf{5}^+$ and $\mathbf{6}^+$, cation radicals are discussed by comparing the EPR spectra and the spin density distribution maps.


*Keywords:* Iridium complexes; Bimetallic complexes; Electrochemistry; Electron transfer; Fluorescence; EPR spectroscopy

## 1. Introduction

Our recent studies [1] dealing with the electronic properties of homobimetallic anthracene-bridged cyclopentadienyl complexes of formula $[L_2M\{C_5H_4CH_2(9,10\text{-anthrylene})CH_2C_5H_4\}ML_2]$ have shown that the 9,10-bis-(methylene)anthracene fragment, i.e. $CH_2(9,10\text{-anthrylene})CH_2$, appears to be a promising bridging ligand for assembling potentially useful molecular devices for electronics and optoelectronics [2] since it, owing to its electronic and conformational properties, may switch on/off the communication between the linked sites. A strong electronic communication occurs indeed between the

* Corresponding author. Tel.: +39 50 2219351; fax: +39 50 2219410.
*E-mail address:* vanni@dcci.unipi.it (G. Ingrosso).

0022-328X/$ - see front matter © 2006 Elsevier B.V. All rights reserved.
doi:10.1016/j.jorganchem.2006.03.017

9,10-anthrylene group and the two cyclopentadienyl$RhL_2$ moieties in the homo-bimetallic derivatives of rhodium(I) having the above formula with $L = C_2H_4$ or CO [1a]. In the case of these compounds, in fact, the oxidation of the two metal centres occurs at different potentials, indicating that a metal–metal interaction exists in the ground state. Furthermore, the EPR of the cation-radicals, i.e. $[L_2Rh\{C_5H_4CH_2(9,10\text{-anthrylene})CH_2C_5H_4\}RhL_2]^{+\bullet}$, which arise from the one-electron oxidation of the above complexes documents clearly that the spin density distribution extends over the whole molecular skeleton and that a long-range interaction exists between the two metal centres. Thus, these cation-radicals are best described as $[Rh^{+1.5}, Rh^{+1.5}]$ average-valence complexes (Class III behaviour) [3] and as such they are *large molecules* [4].

The scenario changes markedly on passing from CO and ethylene, as the ancillary ligands, to *cis*-cyclooctene and 1,5-cyclooctadiene [1b]. In fact, the electrochemical behaviour of such complexes unambiguously shows that the two metal centres (both in the case of rhodium and iridium derivatives) are oxidized at the same potential, thus indicating that they do not interact in the ground state. In addition, EPR spectroscopy documents that no long-range interaction exists between the two metal centres in the corresponding cation-radicals (Class I behaviour) [3].

These observations prompted us to extend our study to the new homobimetallic anthracene-bridged $\eta^5$-cyclopentadienyl derivatives of iridium(I) **3** and **4**.

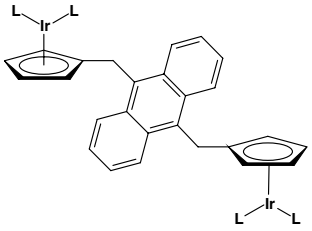


**3**, L = $\eta^2$-$C_2H_4$

**4**, L = CO

Through the comparison of the electronic properties of these compounds with those of the isostructural rhodium(I) derivatives we expected to discover possible differences and analogies between the roles played by the two metals in influencing the photo-physical and electrochemical features of the neutral compounds as well as the electronic properties (EPR) of the corresponding cation radicals. The results of this study are the object of this paper.

## 2. Results and discussion

### 2.1. Preparation of the complexes *3*, *4*, and *5*

The reaction of 9,10-bis[(cyclopentadienylmethyl)thallium(I)]anthracene **2** [1a] with $[IrCl(\eta^2\text{-}C_2H_4)_4]$ and

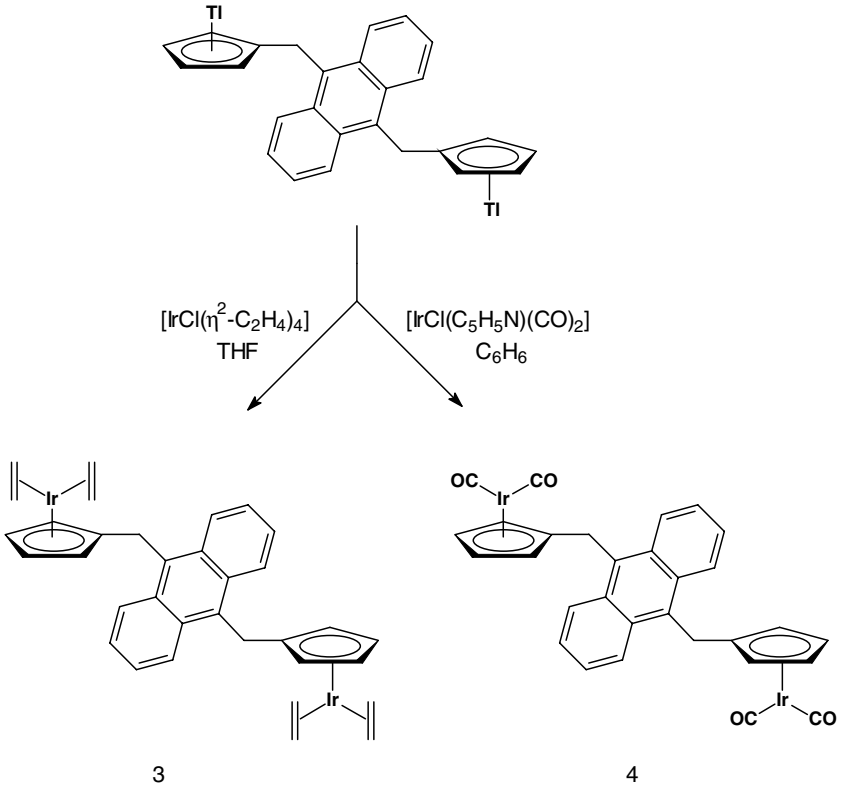


3 4

Scheme 1.

$[IrCl(C_5H_5N)(CO)_2]$ produces the bimetallic derivatives **3** and **4**, respectively, as yellow microcrystalline solids (Scheme 1). Both complexes are sufficiently thermally stable in the solid state to be manipulated at room temperature under dinitrogen without any apparent alteration. Anyway, **4** is significantly more stable than **3**. Notably, the yields obtained in the two cases (31% and 9%, respectively) decrease in the same order. The new complexes were characterized by elemental analysis, $^1$H NMR, mass spectrometry, and, in the case of **4**, also by FT-IR. Well resolved $^1$H NMR were obtained (Table 1) which are consistent with the proposed structures, the observed spectral patterns being in agreement with those observed in the case of the isostructural rhodium(I) derivatives [1a]. The CO stretching frequencies of complex **4** (2027 and 1959 $cm^{-1}$, in benzene), which are practically identical to those of ($\eta^5$-9-anthrylmethylcyclopentadienyl)dicarbonyliridium(I) (**6**) (2027, 1957 $cm^{-1}$, in benzene) [5], result to be slightly lower than those exhibited by $[Ir(\eta^5\text{-}C_5H_5)(CO)_2]$ (**8**) (2037 and 1957 $cm^{-1}$, in benzene) [6], thus showing that the electron-donating power of the anthrylenic-substituted cyclopentadienyl ligand is moderately higher than that of unsubstituted cyclopentadienyl, but lower than that of pentamethylcyclpentadienyl ($[Ir(\eta^5\text{-}C_5Me_5)(CO)_2]$: CO stretching, 2000 and 1925 $cm^{-1}$) [7]. Expectedly, the CO stretching frequencies of the isostructural rhodium(I) derivative, i.e. $[(CO)_2Rh\{C_5H_4CH_2(9,10\text{-anthrylene})CH_2C_5H_4\}Rh(CO)_2]$, occur at slightly higher frequencies (2042 and 1979 $cm^{-1}$, in benzene) [1a].

The ESI-MS (electro-spray ionization mass spectrometry) spectrum of **3** shows a complex pattern of pseudomolecular peaks arising from the presence of the two iridium isotopes ($^{191}$Ir, 37.3%; $^{193}$Ir, 62.7%) as well as from the presence of two iridium centres. Thus, the peaks due to $[M+H]^+$ ($^{193}$Ir,$^{193}$Ir, *m/z* 831), $[M+H]^+$ ($^{193}$Ir, $^{191}$Ir, *m/z* 829), and $[M+H]^+$ ($^{191}$Ir, $^{191}$Ir, *m/z* 827) are observed, along with other peaks due to metal-containing fragments arising from the loss of two or three ethylene molecules and to other unidentified fragments. Attempts to obtain a mass spectrum of **4** by the same technique failed. Instead, by using a particle beam (PB) LC/MS system [8], a good mass spectrum of **4** was obtained under EI conditions, which shows a low intensity complex pattern of molecular peaks: $[M]^+$ ($^{193}$Ir, $^{193}$Ir, *m/z* 830), $[M]^+$ ($^{193}$Ir, $^{191}$Ir, *m/z* 828), and $[M]^+$ ($^{191}$Ir, $^{191}$Ir, *m/z* 826). In addition, are clearly observable the peaks due to metal-containing fragments arising from the loss of one, three, or four CO ligands.

Table 1
$^1$H NMR data for the complexes **3** and **4**[a]

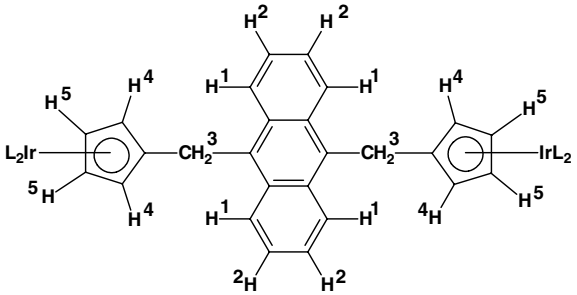


| Complex | $\delta$ (ppm), *J* (Hz) |
|---|---|
| **3** (L = $\eta^2$-$C_2H_4$) | 8.40–8.35 (4H, m, $H^1$), 7.34–7.29 (4H, m, $H^2$), 4.61 (4H, d, $J_{HH}$ 1, $H^5$), 4.51 (4H, d, $J_{HH}$ 1, $H^4$), 4.41 (4H, s, $H^3$), 2.54–2.49 (8H, d, $J_{HH}$ 10, $C_2H_4$), 0.85–0.80 (8H, d, $J_{HH}$ 10, $C_2H_4$) |
| **4** (L = CO) | 8.17–8.12 (4H, m, $H^1$), 7.35–7.29 (4H, m, $H^2$), 4.76 (4H, d, $J_{HH}$ 2, $H^5$), 4.57 (4H, d, $J_{HH}$ 2, $H^4$), 4.34 (4H, s, $H^3$) |

[a] Spectra recorded in $C_6D_6$; s = singlet; m = multiplet; d = doublet.

In the study of the electrochemical behaviour of **3** and **4** (see Section 2.3), it was envisaged the opportunity to compare the electrochemical peculiarities of the bimetallic complexes with those exhibited by the corresponding monometallic 9-anthrylcyclopentadienyl derivatives of iridium(I) **5** and **6**. Complex **6** has already been reported in the literature [5].

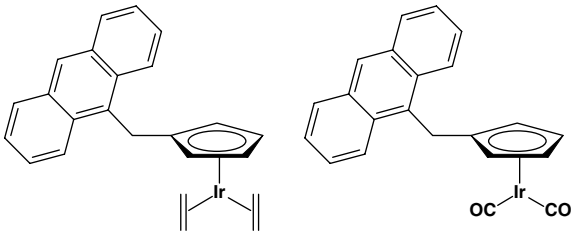


**5** **6**

Complex **5** has now been obtained (27%, yields) by reacting 9-anthrylmethylcyclopentadienylthallium(I) [9] with $[IrCl(\eta^2\text{-}C_2H_4)_4]$ (Eq. (1)), and characterized by elemental analysis, $^1$H NMR, and Turbo-V Ionspray mass spectrometry (see Section 4), as well as by single-crystal X-ray diffractometry.

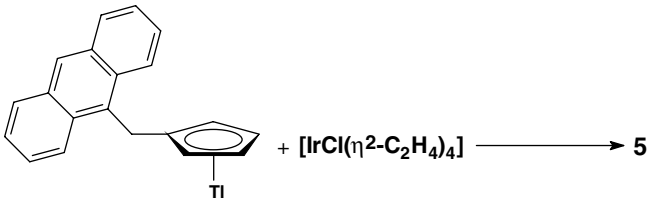


(1)

The molecular structure of **5** is shown in Fig. 1. The asymmetric unit in the crystal structure of **5** consists of two independent molecules approximately related by an inversion centre. However, this pseudo-centre represents only a local symmetry, being placed in an irrational position with respect to the screw axes, which are the only symmetry operators valid for the whole structure. The conformation is very similar to that found in the isostructural rhodium(I) derivative [9], which by chance resembles **5** also having two molecules in the asymmetric unit. Due to the very similar radii of Rh(I) and Ir(I) ions, the same mean distances M–Cp and M–Eth (Cp = cyclopentadienyl centroid; Eth = ethylene centroid) and the same mean angles, Cp–M–Eth and Eth–M–Eth, are observed. The more pronounced difference in the geometry of the two compounds

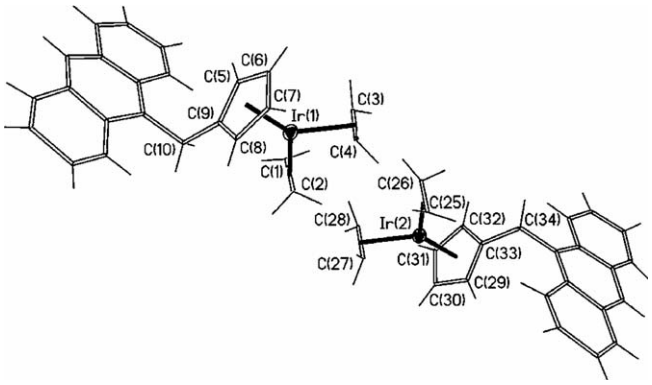


Fig. 1. View of the two independent molecules present in the structure of **5**. Selected bond lengths (Å) and angles (°): Ir(1)–C(1), 2.08(2); Ir(1)–C(2), 2.08(2); Ir(1)–Eth1, 1.96(2); Ir(1)–C(3), 2.09(3); Ir(1)–C(4), 2.11(2), Ir(1)–Eth2, 1.98(1); Ir(1)–Cp1, 1.89(1); Ir(2)–C(25), 2.13(2); Ir(2)–C(26), 2.06(2); Ir(2)–Eth3, 1.97(2); Ir(2)–C(27), 2.11(3); Ir(2)–C(28), 2.10(2), Ir(2)–Eth4, 1.98(1); Ir(1)–Cp2, 1.88(1); Cp1–Ir(1)–Eth1, 134.8(9); Cp1–Ir(1)–Eth2, 129.6(7); Eth1–Ir(1)–Eth2, 95.6(8); Cp2–Ir(2)–Eth3, 132.4(8); Cp2–Ir(2)–Eth4, 133.6(7); Eth3–Ir(2)–Eth4, 94.0(8). Cp and Eth are the centroids of the cyclopentadienyl group and ethylene, respectively.

deals with the dihedral angle formed by the coordinated Cp rings with the corresponding 9-anthryl plane, which is wider in the rhodium(I) compound than in **5**: 110° and 103°, respectively. Finally, a close resemblance may also be found with the only other reported structure of a bis($\eta^2$-ethylene) iridium complex carrying a cyclopentadienyl ligand, i.e. 1-(2-dimethylamino)phenyl-3-(*tert*-butylcyclopentadienyl)bis($\eta^2$-ethylene)iridium(I) [10]. Indeed, the reported geometric data for this compound are very similar to those found for **5**.

### 2.2. Absorption and emission spectroscopic studies

The UV–Vis absorption spectra of **3** and **4** (290–500 nm) are reported in Fig. 2 along with the spectrum of 9-methylanthracene and those of **7** and **8**.

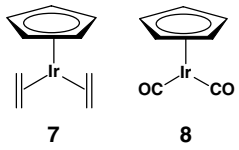


**7** **8**

The spectra of **3** and **4** are characterized by the typical doubly substituted anthracene vibrational structure [11] although they are slightly less resolved than the spectrum of 9-methylanthracene. Moreover, both the spectra exhibit an absorption tail which extends up to 430 nm and 450 nm, respectively, in the case of **3** and **4**. This is evident if one compares the spectra of **3** and **4** with those resulting from the sum of the spectrum of 9-methylanthracene, shifted of about 14 nm towards red, and of the spectra of **7** and **8** considered twice (Fig. 2). The less resolved vibrational structure and the absorption tails are the first indication of the existence of an electronic interaction among the 9,10-anthrylenic chromophore and the two cyclopentadienyl–metal sub-units [12]. The parameters of the last vibrational band and of the preceding minimum of the UV–Vis spectra of **3** and **4** along with those of 9-methylanthracene and of 9,10-bis(cyclopentadienylmethyl)anthracene (**1**) are reported in Table 2. The **r** parameter is related to the resolution of the vibrational structure: the higher the **r** value the higher the spectral resolution. Looking at this parameter, the UV–Vis spectra of complexes **3** and **4** are less resolved than the spectrum of 9,10-bis(cyclopentadienylmethyl)-anthracene (**1**) which is less resolved than the spectrum of 9-methylanthracene, but more resolved than those of the isostructural rhodium compounds. Moreover, the spectrum of the ethylene derivative **3** is less resolved than that of carbonyl complex **4**.

The observed electronic interaction among the sub-units of **3** and **4** is confirmed by the fact that, while 9-methylanthracene and 9,10-bis(cyclopentadienylmethyl)anthracene

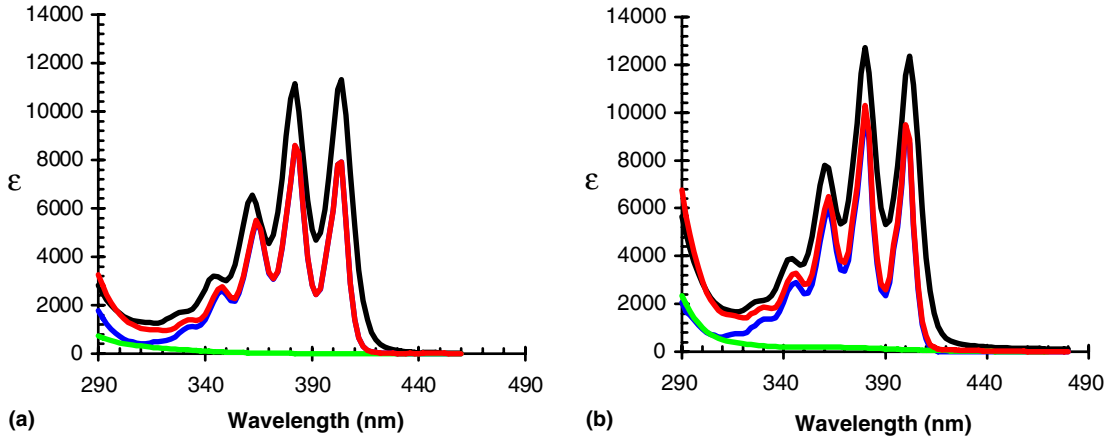


Fig. 2. (a) Comparison of the UV–Vis spectrum of [($\eta^2$-$C_2H_4$)$_2$Ir {$C_5H_4CH_2$(9,10-anthrylene)$CH_2C_5H_4$}Ir($\eta^2$-$C_2H_4$)$_2$] (**3**) (black solid line) with the sum (red solid line) of the spectra of 9-methylanthracene (blue solid line) and of [Ir($\eta^5$-$C_5H_5$)($\eta^2$-$C_2H_4$)$_2$] (**7**) (green solid line) considered twice. (b) Comparison of the UV–Vis spectrum of [(CO)$_2$Ir{$C_5H_4CH_2$(9,10-anthrylene)-$CH_2C_5H_4$}Ir(CO)$_2$] (**4**) (black solid line) with the sum (red solid line) of the spectra of 9-methylanthracene (blue solid line) and of [Ir($\eta^5$-$C_5H_5$)(CO)$_2$] (**8**) (green solid line) considered twice. In both cases the spectrum of 9-methylanthracene is shifted 14 nm towards red.

Table 2
UV–Vis absorption data for 9-methylanthracene, 9,10-bis(cyclopentadienyl-methyl)anthracene (**1**), and complexes **3** and **4**[a]

| Compound | Absorption | | | | |
|---|---|---|---|---|---|
| | $\lambda_1$ | $\varepsilon_1$ | $\lambda_{min}$ | $\varepsilon_{min}$ | **r** ($\varepsilon_1/\varepsilon_{min}$) |
| 9-Methylanthracene | 390 | 9300 | 378 | 2600 | 3.60 |
| 9,10-Bis(cyclopentadienylmethyl)anthracene (**1**) | 404 | 11000 | 390 | 4600 | 2.39 |
| $[(\eta^2\text{-}C_2H_4)_2Ir\{C_5H_4CH_2(9,10\text{-anthrylene})CH_2C_5H_4\}Ir(\eta^2\text{-}C_2H_4)_2]$ (**3**) | 404 | 11300 | 392 | 5000 | 2.26 |
| $[(CO)_2Ir\{C_5H_4CH_2(9,10\text{-anthrylene})CH_2C_5H_4\}Ir(CO)_2]$ (**4**) | 402 | 12500 | 390 | 5400 | 2.31 |
| $[(\eta^2\text{-}C_2H_4)_2Rh\{C_5H_4CH_2(9,10\text{-anthrylene})CH_2C_5H_4\}Rh(\eta^2\text{-}C_2H_4)_2]$[b] | 404 | 8500 | 394 | 4780 | 1.78 |
| $[(CO)_2Rh\{C_5H_4CH_2(9,10\text{-anthrylene})CH_2C_5H_4\}Rh(CO)_2]$[b] | 404 | 14000 | 394 | 6520 | 2.15 |

[a] All spectra were recorded in benzene solution. $\lambda$ are in nm; $\varepsilon$ is given as $M^{-1}\,cm^{-1}$.
[b] Ref. [1b].

(**1**) both show a very intense emission spectra, when they are excited at wavelengths ranging from 333 nm to 383 nm, the fluorescence emission of **3** and **4** is almost completely quenched, under the same conditions. The very low residual fluorescence observed (<1%) is quite probably due to traces of fluorescent impurities which may be present even after the very accurate chromatographic purification of the complexes.

The UV–Vis absorption spectra of the monometallic complexes **5** and **6** (290–500 nm) are quite similar to those exhibited by **3** and **4** and are in line with previous observations [5,9]: in both cases the spectra are slightly less resolved than the spectrum of 9-methylanthracene, taken as the reference compound, and both the spectra exhibit an absorption tail. Furthermore, while 9-anthrylcyclopentadiene is an efficient light-emitting molecule when excited at 365 nm [9], **5** and **6** are very poor luminescent compounds, although the residual fluorescence observed (<5%) is slightly higher than that measured for **3** and **4**.

### 2.3. Electrochemical studies

The CV curve for a 1.0 mM of **3** in THF, obtained under strictly aprotic conditions, is shown in Fig. 3a. In the region of negative potentials, a reversible one-electron reduction with $E_{1/2} = -1.89$ V, likely involving the 9,10-anthrylenic unit, is observed followed, at more negative potentials, by an irreversible reduction peak ($E_p = -2.6$ V;

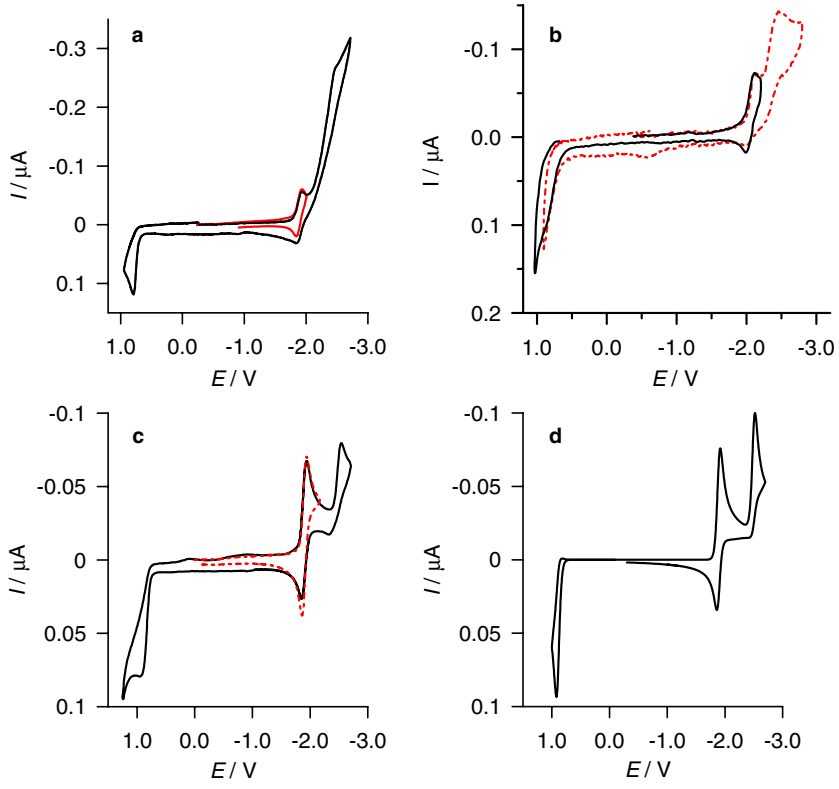


Fig. 3. Cyclic voltammetric curves of (a) 1 mM of **3**, (b) 1 mM of **4** and (c) 1 mM of **5**, 0.05 M TBAH, THF solutions; scan rate: 0.5 V/s; working electrode, Pt disc ($r = 65$ µm); $T = 22$ °C. (d) Digital simulation of cyclic voltammetric curve shown in (c): simulation parameters: $E°$: +0.90 (oxidation); −1.89 and −2.50 V (reductions) (Nernstian processes). Rate constants of follow-up chemical reactions coupled to oxidation and second reduction (EC mechanisms, see text): $10^3\ s^{-1}$.

at 5 V/s) displaying peak currents largely exceeding that of first peak. A similar reduction pattern is observed for the monometallic complex **5**, investigated under similar conditions (Fig. 3c and Table 3). No such reduction processes are instead detected in the case of the model complex, $[Ir(\eta^5\text{-}C_5H_5)(\eta^2\text{-}C_2H_4)_2]$ (**7**), thus substantiating the identification of the two reduction processes involving both **3** and **5** with the subsequent reductions of the anthrylic unit. The irreversibility of the second reduction peak in both complexes is still observed at scan rates as high as 200 V/s, and can be associated with the occurrence of relatively fast follow-up chemical reactions (EC mechanism) [13a] as suggested by the observed shift of the peak to more negative potentials by approximately 30 mV for any 10-fold increase of scan rate. Furthermore, the very large current of the second reduction of bimetallic complex **3** would also suggest that such a process triggers an electrocatalytic process, likely associated with the strong basicity of 9,10-anthrylenic dianion, analogously to the voltammetric behaviour of several polypyridine ligands, investigated under similar conditions [14].

In the region of positive potentials, the CV curve of the bimetallic complex **3** displays an irreversible anodic peak ($E_p = 0.80$; at 0.5 V/s). By comparison with the first one-electron reduction of the 9,10-anthrylenic unit, such a peak corresponds to a two-electron oxidation peak, resulting from the superimposition of two one-electron oxidation processes occurring at close potentials. By contrast, in the CV curve of the monometallic complex **5** (Fig. 3c), a similar process, located at $E_p = 0.89$ V (at 0.5 V/s), corresponds instead to a single one-electron oxidation process. It is therefore inferred that the oxidation processes in **3** and **5** are mainly localized onto the metal centres.

The CV curve for a 1.0 mM THF solution of **4** is shown in Fig. 3b. In the region of negative potentials two reduction peaks are observed: the first peak corresponds to a one-electron reversible process with $E_{1/2} = -2.05$ V, while the second peak is associated with a two-electron irreversible process ($E_p = -2.46$ V). On comparison with the corresponding mononuclear complex **6**, whose CV behaviour under similar experimental conditions has previously been reported (a reversible one-electron reduction followed by an irreversible one, at −2.09 V and −2.52 V, respectively) [5], the first peak can be attributed to the first reversible reduction of the 9,10-anthrylenic group and the two-electron peak to the reduction of the two metal centres. Such an attribution of the latter peak is confirmed by comparison with the CV curve of the model compound, $[Ir(\eta^5\text{-}C_5H_5)(CO)_2]$ (**8**) [5]. A totally reversible behaviour is not attained even at scan rates as high as 200 V/s, while the potentials of the second peak shifted to more negative values by approximately 30 mV for a 10-fold increase of scan rate, suggesting that the irreversibility is associated with the occurrence of a fast chemical reaction following the reduction process (EC mechanism) [13a]. Whenever the forward scan includes the two-electron metal-centred reduction peak, an irreversible anodic peak, located at ca. −0.6 V, is also observed in the reverse scan. Such a peak is attributed to the oxidation of the product(s) deriving from the above follow-up chemical reaction. A similar irreversible peak at ca. −0.6 V has been observed in the CV behaviour of the corresponding monometallic complex **6** [5]. In the positive potential region, an irreversible anodic peak is observed, partly superimposed to the solvent-electrolyte discharge current. By comparison with the anthrylic-centred reduction peak, such a peak (with $E_p = 0.81$ V) would correspond to a two-electron transfer and is therefore associated with the oxidation of the metal centres. Also in this case the agreement with the behaviour of the monometallic complex **6** is good (a one-electron process with $E_p = 0.85$ V) [5]. A (more) reversible behaviour could not be observed even at scan rates as high as 200 V/s. Thus, on the basis of the scan rate dependence of peak potential, we conclude that the irreversibility is associated with the occurrence of a fast chemical degradation of the electrochemically generated radical cation(s).

The electrochemical behaviour exhibited by complexes **3** and **4** in the positive potentials region clearly shows that the dicationic species formed upon their electrochemical oxidation are chemically unstable in the time scale of cyclic voltammetry. The reactivity of the oxidised complexes (with lifetimes typically less than milliseconds, see digital simulation of the CV curve in Fig. 3) has likely to be associated with the presence of a high concentration of hexafluorophosphate anions (supporting electrolyte) whose nucleophilicity towards highly reactive cations, such as for instance $C60^{\bullet+}$, has recently been pointed out [13b,13c]. The effect of the fast irreversible chemical reactions following the first and, more importantly, the second oxidation may in fact explain, according to an ECEC mechanistic scheme [13a], the apparent coincidence of the oxidation potentials of the two CpIr moieties in **3** and **4**. In other words, such a coincidence of the two metal-centred oxidations would originate from kinetic effects on the CV morphology rather than reflecting the thermodynamic stability of dicationic vis-à-vis cationic species. On

Table 3
CV parameters for compounds **3**–**6**[a]

| Compound | Oxidation | Reduction | $-\Delta G^0_{CR}$ (eV)[e] | $-\Delta G^0_{CS}$ (eV)[f] |
|---|---|---|---|---|
| **3** | 0.80[b,c] (0.82) | −1.89[d]; −2.60[b] | 3.1 | 0.1 |
| **5** | 0.89[b] (0.90) | −1.90[d]; −2.53[b] | 3.1 | 0.1 |
| **4** | 0.81[b,c] (0.83) | −2.05[d]; −2.46[b,c] | 3.3 | ~0 |
| **6**[g] | 0.85[b] (0.86) | −2.09[d]; −2.52[b] | 3.2 | ~0 |

[a] V vs. SCE, $T = 25$ °C.
[b] $E_p$, irreversible process.
[c] Two-electron process.
[d] $E_{1/2}$.
[e] Driving force for charge recombination from CS state.
[f] Driving force for the photoinduced intramolecular charge transfer (reductive quenching, see text). A correction to the CS state energy of 0.2 eV was introduced for taking into account ion–solvent interactions (see text; Ref. [15]).
[g] Data taken from Ref. [5]. In parentheses: $E^\circ$ values obtained by digital simulation of the CV curves (see text).

the other hand, on the basis of the present experimental results, the hypothesis that the single two-electron anodic peak be instead indicative of the absence of sizeable interactions between the metal moieties cannot totally be ruled out.

The strong quenching of 9,10-anthrylene fluorescence observed for **3** and **4** may be explained assuming that an intramolecular charge transfer between the excited 9,10-anthrylenic moiety and the metal-containing moieties may occur, which generates a charge-separated (CS) state (Scheme 2). The thermodynamic requirement that such a process be exoergonic is quantitatively verified by the evaluation of the driving force for the photoinduced charge separation process, $-\Delta G^0_{CS} = E_{00} + \Delta G^0_{CR}$, where $E_{00}$ is the excited state energy of the anthrylene-based chromophore (~3.2 eV) and $\Delta G^0_{CR}$ is given by the following equation:

$$-\Delta G^0_{CR} = E_{1/2}(D^+/D) - E_{1/2}(A/A^-) + \Delta G_s \quad (2)$$

Here electron donor ($D^+/D$) are the $CpIrL_2$ moieties while the acceptor ($A/A^-$) is the chromophore itself (reductive quenching). The correction term $\Delta G_s$ accounts both for ion-pair electrostatic interaction in the CS state and for energy correction when, as in the present case, electrochemical and photo-physical data respectively were obtained in different solvents [15]. The calculation of the above driving force values requires the knowledge of the standard (or halfwave) potentials relative to oxidation of donors and reduction of acceptors. While the latter is known in all the systems investigated in the present work [the reduction of the 9,10-anthrylenic moiety is invariably reversible, both chemically and electrochemically, and the corresponding $E_{1/2}$ values are therefore obtained as average of peak potentials (see Section 4)], the $E_{1/2}$ values relative to metal-centred oxidations cannot be directly available because of the irreversibility of such processes, and were therefore evaluated by digital simulation of the CV curves. The simulation is based on the working hypothesis that, as anticipated above, oxidation of metals, as well as the second reduction of the anthryl group, would trigger a fast chemical degradation of the resulting radical cation, or dianion, according to the so-called EC mechanism. An example of simulated curve, calculated under the same conditions of Fig. 3c, is shown in Fig. 3d and displays a very good agreement with the experimental curve. The thermodynamic $E_{1/2}$ values relative to the oxidation of the metal centres for all the species thus obtained are reported in Table 3, along with the driving force values for the forward (photoinduced) and backward (thermal) intramolecular electron transfer.

In both mono and bimetallic species, the charge separated state is highly energetic and the photo-induced charge separation process results therefore to be only slightly exoergonic. On the other hand, the corresponding charge recombination of the CS state to the ground state is highly exoergonic. It is therefore likely that, while the forward charge separation process is located in the favourable normal Marcus region (thus explaining the strong quenching of the chromophore excited state), charge recombination processes is located in the Marcus inverted region, i.e.,

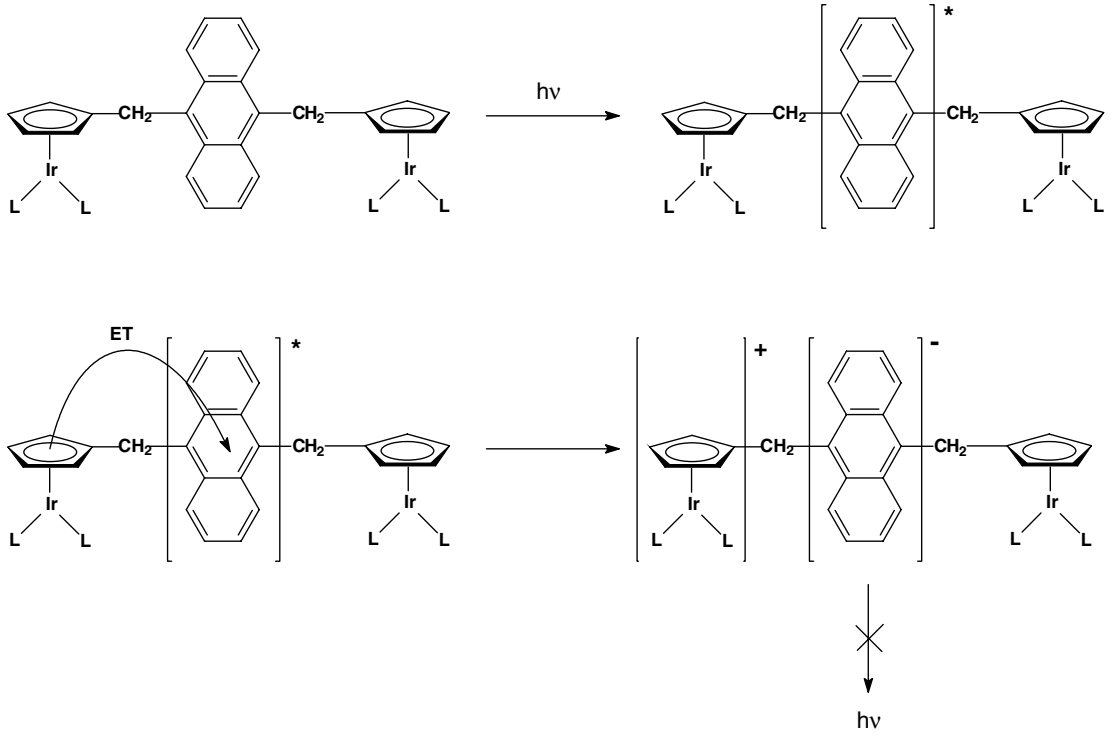


Scheme 2.

where $\Delta G^0_{CR} < -\lambda$, whence relatively long lifetimes of the CS states might be expected.

### 2.4. Chemical oxidation of complexes 3–6: EPR studies and DFT calculations

These reactions were carried out following the already described procedure [1,5], using the 1,1,1,3,3,3-hexafluoropropan-2-ol/$CH_2Cl_2$ 1:1 (v/v) mixture as the reaction medium. A preliminary investigation on the chemical oxidation of **3** and **4** led us to use successfully PIFA for the oxidation of **3** and TTFA for the oxidation of **4**. The reactants were made to come into contact at low temperature (−80 °C) into the cavity of an EPR spectrometer. Then, the temperature was gradually raised until a signal appeared. In the case of the oxidation of **3**, no signal appeared at temperatures lower than −30 °C. At this temperature, the spectrum ($\Delta H_{pp} = 0.42$ G, $g_{iso} = 2.0031$), shown in Fig. 4, was recorded which is consistent with the kinetically labile radical cation $\mathbf{3}^+$ exhibiting a spin delocalization confined to three sets of protons ($a^1_H = 3.83$ G, 4H; $a^2_H = 2.61$ G, 4H; $a^3_H = 1.31$ G, 4H) and to two $^{191,193}$Ir centres ($I = 3/2$, 37.3% and 62.7% natural abundance) ($a_{Ir} = 0.95$ G, 2Ir). The hyperfine coupling constants and line-widths were obtained by computer simulation of the experimental spectrum.

The most intense signal arises from the interaction of the unpaired electron with five sets of protons ($a^1_H = 3.37$ G, 4H; $a^2_H = 1.67$ G, 4H; $a^3_H = 1.47$ G, 4H; $a^4_H = 1.31$ G, 4H; $a^5_H = 0.41$ G, 4H) and with two iridium nuclei ($a_{Ir} = 0.90$ G, 2Ir). The simulation of the other signal shows, instead, that spin delocalization involves three sets of protons ($a^1_H = 2.67$ G, 4H; $a^2_H = 2.63$ G, 4H; $a^3_H = 1.00$ G, 2H) and only one iridium centre ($a_{Ir} = 1.51$ G, 1Ir).

Unfortunately we did not succeed in obtaining more resolved EPR spectra for the cation radicals $\mathbf{3}^+$ and $\mathbf{4}^+$. Thus, with the aim to substantiate the above simulations, we decided to resort to DFT calculation of the spin density distribution of the above cation radicals, which indeed allowed a theoretical evaluation of the isotropic hyperfine coupling constants for the various hydrogen atoms in $\mathbf{3}^+$ and $\mathbf{4}^+$ and gave a further insight into their structure. DFT data were obtained by using the SPARTAN program ('02 Version) [16] and adopting the hybrid B3LYP density functional model that uses the Becke's three-parameter functional [17] with the non-local correlation term provided by the Lee–Yang–Parr expression [18], adopting the 6-31G** base functions set, which is appropriate for calculations of split-valence-plus-polarization quality. For the sake of clarity only the negative spin density is represented in the maps of Fig. 5. Anyway, the positive and negative

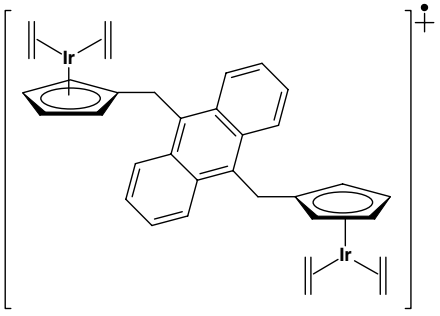


$\mathbf{3}^+$

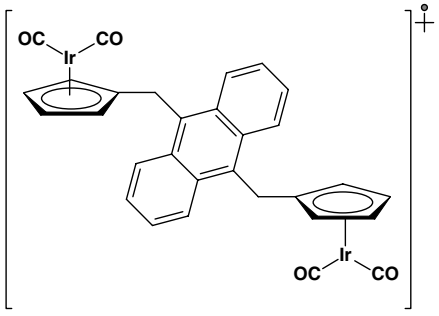


$\mathbf{4}^+$

When the dicarbonyl derivative **4** was reacted with TTFA, the EPR spectrum shown in Fig. 4 appeared, at −15 °C. As can be observed, such a spectrum reveals a moderate asymmetry, the right side being larger and less resolved than the left one. Indeed, the computer simulation of the spectrum (Fig. 4) accounts for the superimposition of two signals associated with a largely prevalent (96%) radical species ($\Delta H_{pp} = 0.3$ G, $g_{iso} = 2.006$) and to another one which is much less abundant (4%) ($\Delta H_{pp} = 0.3$ G, $g_{iso} = 2.007$). Computer simulation of the spectrum reveals that the signals are due to two radical species having the same skeletal structure, i.e. that of the cation radical $\mathbf{4}^+$, but different spin delocalization.

spin density distribution shows clearly that, in the optimized geometry, the unpaired electron delocalizes over the whole molecular skeleton both in the case of $\mathbf{3}^+$ and $\mathbf{4}^+$. When comparing the theoretical and experimental isotropic hyperfine coupling constants, the limited basis set used, the influence of the solvent, as well as the vibrational and environmental effects should be taken into account in the calculation to produce accurate results. Since it is hard to asses the importance of such effects, a semi-empirical extrapolation procedure [19] has been adopted to correct the theoretical values and compare them with the experimental ones. Interestingly, the calculated isotropic hyperfine coupling constants for $\mathbf{3}^+$ and $\mathbf{4}^+$ (Table 4) are in a

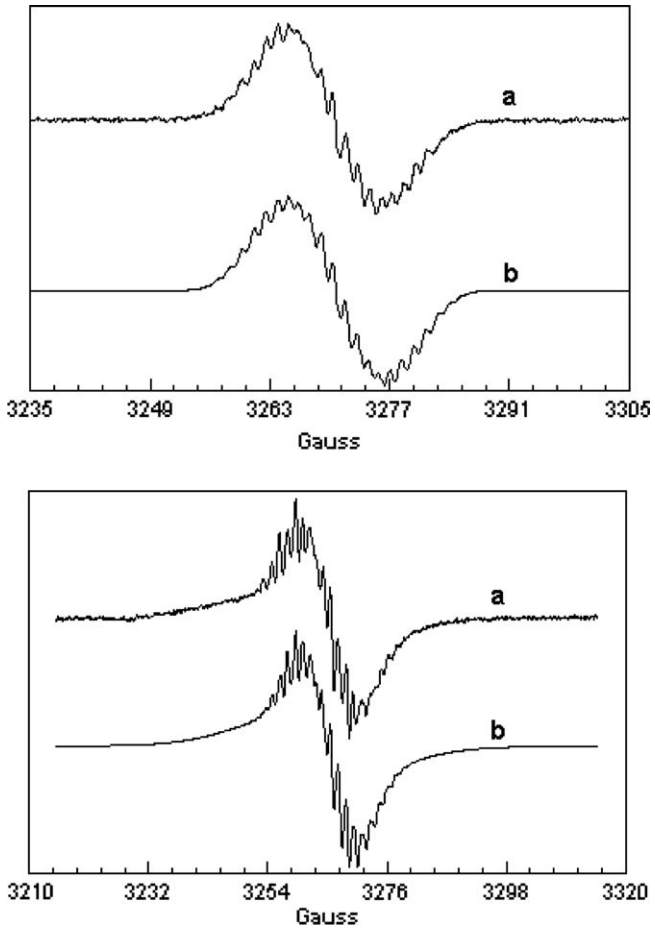


Fig. 4. Experimental (a) and simulated (b) EPR (X-band) spectra of the radical cations $\mathbf{3}^{+}$, $T = 243$ K (up) and $\mathbf{4}^{+}$, $T = 258$ K (down).

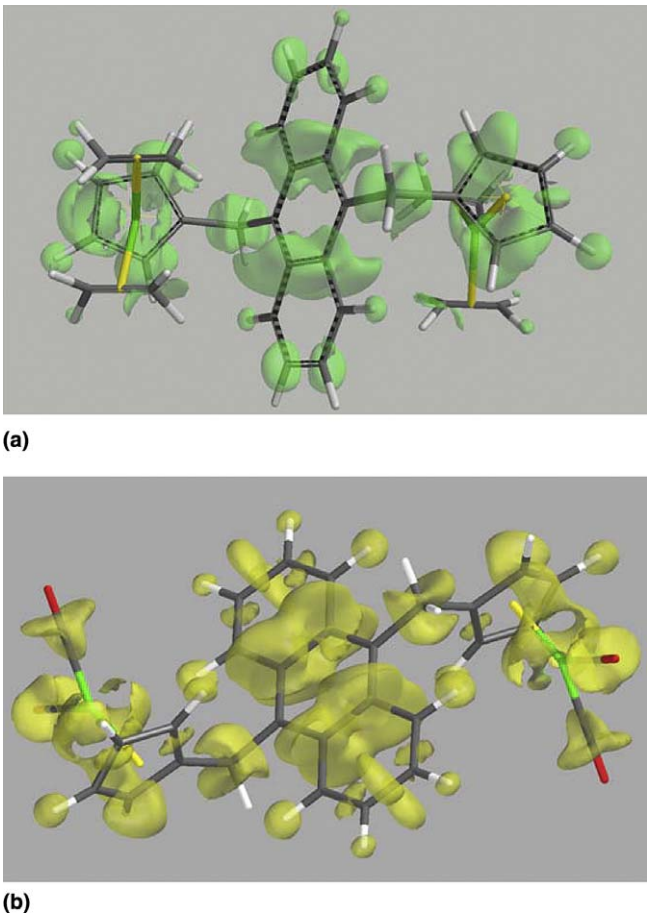


Fig. 5. Spin density surface of the radical cations $\mathbf{3}^{+}$ (−0.0001 electron/a.u.$^3$) (a) and $\mathbf{4}^{+}$ (−0.0001 electron/a.u.$^3$) (b).

remarkable accordance with those obtained by computer simulation of the experimental spectra of Fig. 4. Thus, according to the EPR spectra and DFT calculations, the two iridium centres of $\mathbf{3}^{+}$ and $\mathbf{4}^{+}$ are electronically coupled and the description of $\mathbf{3}^{+}$ and $\mathbf{4}^{+}$ as average-valence [$Ir^{+1.5}$, $Ir^{+1.5}$] complexes is more appropriate, although spin density extends mainly over the 9,10-anthrylene skeleton and much less over the metal centres. In this connection, it must be underlined that completely different EPR spectra are observed in the case of mixed-valent species of the type [$Ir^{+1}$, $Ir^{+2}$] [20] and [$Ir^{+2}$, $Ir^{+3}$] [21] with direct metal–metal interaction, in agreement with the existence of a very high spin-orbit coupling constant of the metal.

Some remarkable differences are observed between $\mathbf{3}^{+}$ and $\mathbf{4}^{+}$, dealing either with the geometry or with the spin density distribution. Indeed, $\mathbf{3}^{+}$ and $\mathbf{4}^{+}$ have quite different molecular geometries, at the energy minimum (Fig. 5). In the case of the cation $\mathbf{3}^{+}$ (L = $\eta^2$-$C_2H_4$), the two cyclopentadienylIr($\eta^2$-$C_2H_4$)$_2$ moieties assume a *transoid* conformation respect to the 9,10-anthrylene plane with both the metal centres facing the aromatic system (Fig. 6a), as already observed in the case of the isostructural rhodium cation radical [1a]. In the case of $\mathbf{4}^{+}$ (L = CO), the two cyclopentadienylIr(CO)$_2$ moieties assume again a *transoid* conformation respect to the 9,10-anthrylene plane, but now the iridium centres do not face the anthrylenic plane, the Cp plane and the anthrylene plane forming a dihedral

Table 4
Hyperfine coupling constants for the cation radicals $\mathbf{3}^{+}$ and $\mathbf{4}^{+}$

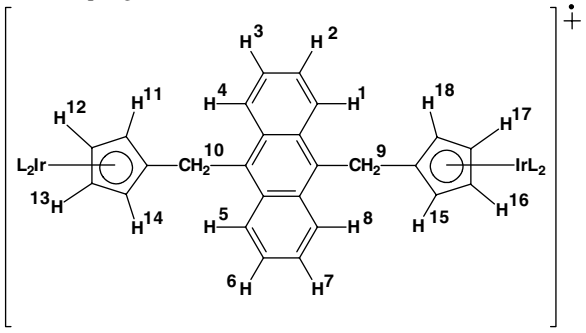


| Nuclei | Calculated and (experimental) hyperfine coupling constants (G) | |
|---|---|---|
| | $\mathbf{3}^{+}$ (L = $\eta^2$-$C_2H_4$) | $\mathbf{4}^{+}$ (L = CO) |
| $H^{12}$, $H^{13}$, $H^{16}$, $H^{17}$ | −3.9 (3.83) | −1.4 (1.47) |
| $H^{1}$, $H^{4}$, $H^{5}$, $H^{8}$ | −2.5 (2.61) | −1.6 (1.67) |
| $H^{2}$, $H^{3}$, $H^{6}$, $H^{7}$ | −1.2 (1.31) | −1.3 (1.31) |
| $H^{11}$, $H^{14}$, $H^{15}$, $H^{18}$ | – (–) | −0.4 (0.41) |
| $H^{9}$(2H), $H^{10}$ (2H) | – (–) | 3.3 (3.37) |

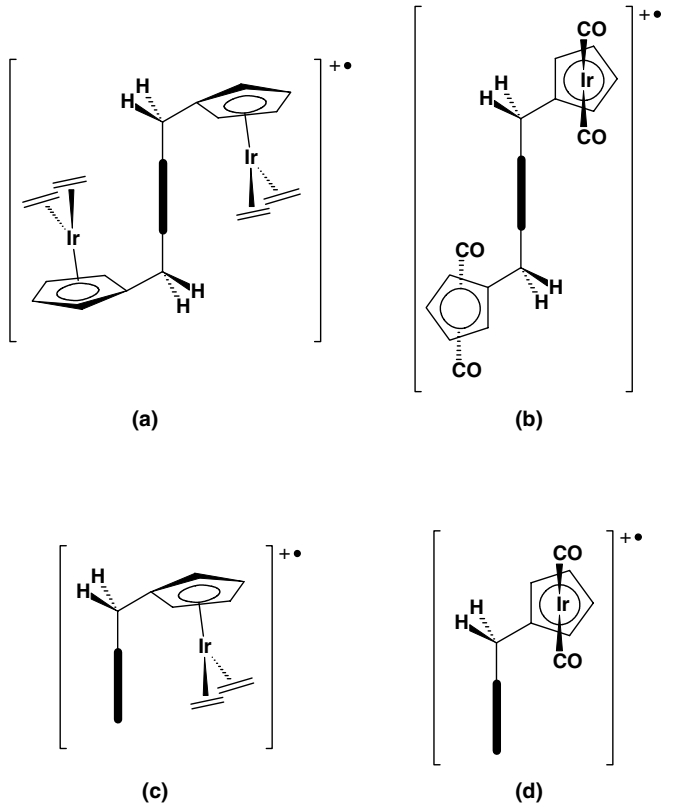


Fig. 6. Schematic representation of the conformation of the cation radicals $\mathbf{3}^+$ (a), $\mathbf{4}^+$ (b), $\mathbf{5}^+$ (c), and $\mathbf{6}^+$ (d) drawn looking along the anthracenic plane profile (▬).

angle of 90° (Fig. 6b). The reasons why $\mathbf{3}^+$ and $\mathbf{4}^+$ have different geometry are not obvious. Anyway, since different conformations cause different spin distributions, it seems particularly interesting the fact that while the spin delocalization does not extend over the methylene group in the case of $\mathbf{3}^+$, it is quite high in the case of $\mathbf{4}^+$, as indicated by the value of the hyperfine coupling constants with the methylenic protons (Table 4). This could suggest that the electronic communication within the whole molecular skeleton occurs through different ways in $\mathbf{3}^+$ and $\mathbf{4}^+$. In the case of $\mathbf{3}^+$, as already pointed out for the isostructural rhodium derivative [1a], the d-electrons of the metal centres, located in π-symmetry orbitals, can overlap with the π-orbitals of the 9,10-anthrylene fragment; therefore, they are delocalized across the connecting ligand and between the two metal centres. In the case of $\mathbf{4}^+$, hyperconjugation seems to be the stabilizing interaction that results from the interaction of the electrons in methylene σ-bonds with the adjacent π-orbitals to give an extended molecular orbital, by virtue of which the odd electron is evenly delocalized over the whole metal–bridge–metal system.

As reported at the beginning of this section, the EPR spectrum of $\mathbf{4}^+$ has been interpreted in terms of the superimposition of two signals. Evidently all the above discussion accounts for the electronic properties of the most abundant radical species, the other one showing a completely different spin distribution (see above). It cannot be ruled out that this last radical is a transient species that converts into the most abundant one, the conversion implying a conformational transformation and then a different spin distribution [22]. A similar scenario has been observed just in the case of the isostructural rhodium derivative $[(CO)_2Rh\{C_5H_4CH_2(9,10\text{-anthrylene})CH_2C_5H_4\}Rh(CO)_2]^+$ [1a].

On the base of the above results it appeared interesting to compare the electronic and conformational peculiarities of the bi-metallic cation radicals $\mathbf{3}^+$ and $\mathbf{4}^+$ with those of the mono-metallic ones, $\mathbf{5}^+$ and $\mathbf{6}^+$. The cation $\mathbf{6}^+$, obtained by oxidation of **6** by TTF, has already been described along with its EPR spectrum [5]. By reacting **5** with TTFA in a 1,1,1,3,3,3-hexafluoropropan-2-ol/$CH_2Cl_2$ 1:1 (v:v) mixture, the EPR spectrum ($\Delta H_{pp} = 0.9$ G, $g_{iso} = 2.0030$) shown in Fig. 7 was recorded, at −30°, that, on the base of computer simulation, is associated with the cation $\mathbf{5}^+$.

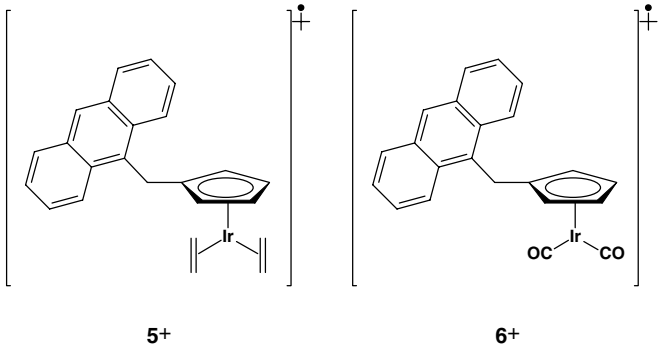


Compound $\mathbf{5}^+$ exhibits a spin delocalization confined to four sets of protons ($a^1_H = 6.26$ G, 4H; $a^2_H = 3.30$ G, 4H; $a^3_H = 2.77$ G, 2H; $a^4_H = 1.59$ G, 1H) and to the iridium centre ($I = 3/2$) ($a_{Ir} = 2.41$ G). The spin density distribution maps for $\mathbf{5}^+$ and $\mathbf{6}^+$ (Fig. 8) were obtained by DFT calculation. Once again, the calculated isotropic

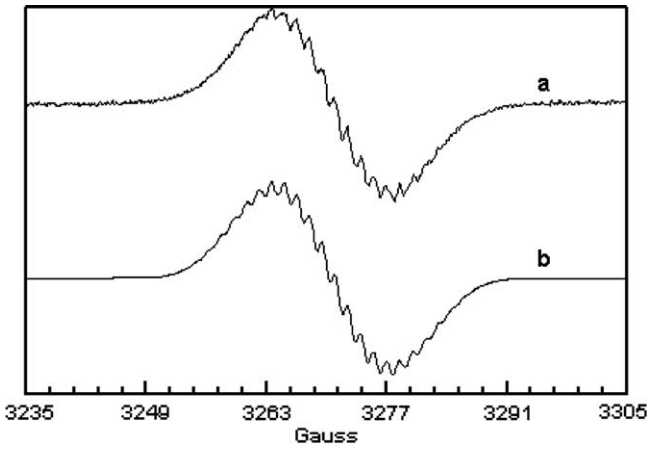


Fig. 7. Experimental (a) and simulated (b) EPR (X-band) spectra of the radical cations $\mathbf{5}^+$ ($\Delta H_{pp} = 0.9$ G, $g_{iso} = 2.0030$; $T = 243$ K).

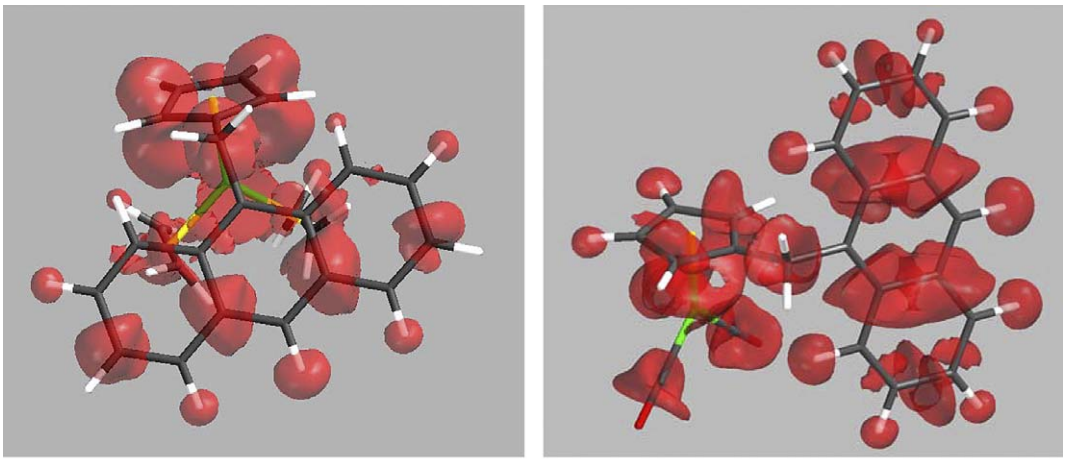


Fig. 8. Spin density surface (−0.0001 electron/a.u.$^3$) of the radical cations $\mathbf{5}^+$ (a) and $\mathbf{6}^+$ (b).

hyperfine coupling constants (Table 5) are in a remarkable accordance with those obtained by computer simulation of the experimental spectra of $\mathbf{5}^+$ (Fig. 7) and $\mathbf{6}^+$ [5]. Furthermore, on analogy with the bimetallic cation $\mathbf{3}^+$, no spin density extends over the methylene group of $\mathbf{5}^+$ and the conformation (Fig. 6c) of such a cation resembles that exhibited by $\mathbf{3}^+$ as well as by other mono-metallic rhodium cation radicals having the same skeletal structure [5], so as the conformation of the mono metallic cation radical $\mathbf{6}^+$ (Fig. 6d) is absolutely similar to that of the bimetallic cation $\mathbf{4}^+$. Moreover, also in the case of $\mathbf{6}^+$ the spin delocalization extends over the methylene group.

Table 5
Hyperfine coupling constants for the cation radicals $\mathbf{5}^+$ and $\mathbf{6}^+$

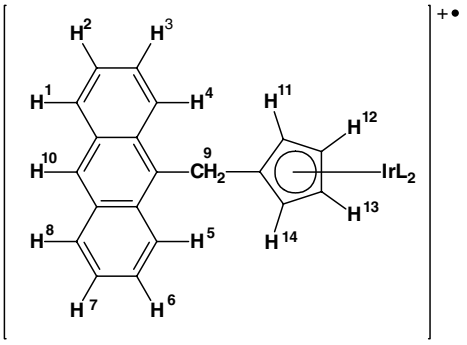


| Nuclei | Calculated and (experimental) hyperfine coupling constants (G) | |
|---|---|---|
| | $\mathbf{5}^+$ (L = $\eta^2$-$C_2H_4$) | $\mathbf{6}^+$ (L = CO)[a] |
| $H^{10}$ | −6.1 (6.26) | −5.1 (5.04) |
| $H^1$, $H^8$ | −2.6 (2.77) | −2.8 (2.88) |
| $H^3$, $H^6$ | −2.6 (2.77) | −1.5 (1.45) |
| $H^4$, $H^5$ | −1.4 (1.59) | −3.0 (2.94) |
| $H^2$, $H^7$ | +1.4 (1.59) | −1.3 (1.38) |
| $H^{12}$, $H^{13}$ | −3.2 (3.30) | −1.6 (1.55) |
| $H^9$ (1H) | – (–) | +1.0 (0.95) |

[a] Experimental data taken from Ref. [5].

## 3. Concluding remarks

The UV–Vis spectra of the bimetallic anthracene-bridged derivatives of iridium(I), [$L_2Ir\{C_5H_4CH_2$(9,10-anthrylene)$CH_2C_5H_4\}IrL_2$] (**3**) (L = $\eta^2$-$C_2H_4$) and **4** (L = CO), indicate of the existence of electronic communication between the 9,10-anthrylene moiety and the cyclopentadienylIr$L_2$ moieties. Accordingly, while 9,10-bis(cyclopentadienylmethyl)anthracene (**1**) is an efficient light-emitting molecule, the fluorescence of the anthrylene group is totally quenched in **3** and **4**, which is much probably due to the occurrence of an intramolecular electron transfer from one cyclopentadienylM$L_2$ moiety to the excited 9,10-anthrylene group, a process that, on the base of the electrochemical data, is justified on a thermodynamic grounding. All these facts are perfectly in agreement with previous observations concerning the isostructural rhodium(I) derivatives, [$L_2Rh\{C_5H_4CH_2$(9,10-anthrylene)$CH_2C_5H_4\}RhL_2$] (L = $\eta^2$-$C_2H_4$; L = CO) [5]. Nevertheless, significant differences exist between the iridium(I) and rhodium(I) complexes (Scheme 3). First of all, the electrochemical behaviour of **3** and **4** shows that the two metal centres are oxidized at the same potential, thus indicating that they do not interact in the ground state. Instead, the oxidation of the two metal centres occurs at different potentials in the case of the isostructural rhodium(I) derivatives, thus indicating that a metal–metal interaction exists in the ground state.

The one-electron chemical oxidation of **3** and **4** leads to the cation radicals $\mathbf{3}^+$ and $\mathbf{4}^+$. These, as well as the isostructural rhodium derivatives [1a], are best described as fully delocalized average-valence [$M^{+1.5}$, $M^{+1.5}$] complexes (Class III behaviour [3]), on the base of their EPR spectra. The DFT calculation of the spin distribution for the rhodium and iridium cation radicals points out interesting details. In fact, while $\mathbf{3}^+$ (L = $\eta^2$-$C_2H_4$) and the rhodium cation radicals have the same geometry, at the calculated energy minimum, which makes the two metal centres to

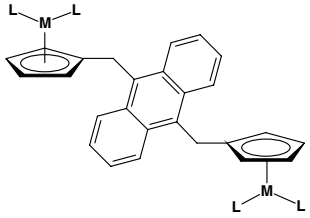


**Rhodium derivatives**
(L = $\eta^2$-$C_2H_4$ or L = CO)

*The rhodium centres are oxidized at different potentials: they **do** communicate in the ground state*

**Iridium derivatives**
(L = $\eta^2$-$C_2H_4$ or L = CO)

*The iridium centres are oxidized at the same potential: they **do not** communicate in the ground state*

**Class III behavior**

**Class I behavior**

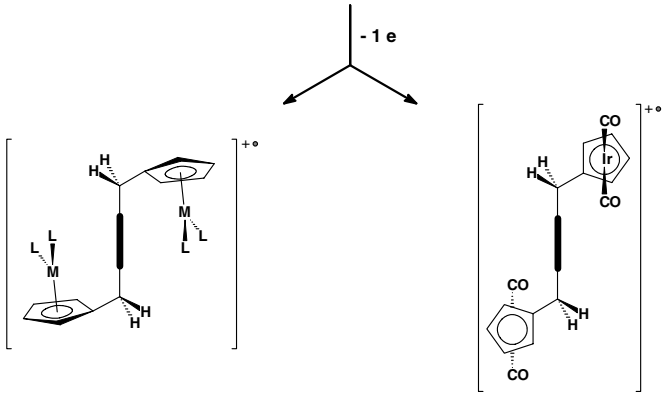


M = Rh (L = $\eta^2$-$C_2H_4$ or L = CO)

**3**$^+$ M = Ir (L = $\eta^2$-$C_2H_4$)

**4**$^+$

*Spin delocalization over the metal-bridge-metal system, which is **low (rhodium) or absent (iridium) over the methylene group**, is suggested to imply an interaction of metal* d*-electron in* ρ *symmetry with the* ρ*-orbitals of the bridging fragment*

*Spin delocalization over the metal-bridge-metal system, which is **very high over the methylene group**, is suggested to imply hyperconjugation of the electrons in methylene* υ*-bonds with the adjacent* p*-orbitals*

**average-valence [$M^{+1.5}$, $M^{+1.5}$] compounds**

**Class III behavior**

Scheme 3.

face the 9,10-anthrylene plane (Scheme 3), **4**$^+$ (L = CO) has a different conformation arising from the fact that both the planes of the two Cp form a dihedral angle of 90° with the plane of 9,10-anthrylene group (Scheme 3). An important consequence of this seems to be the fact that spin delocalization extends also over the methylene bridge (high hyperfine spin-hydrogen coupling constant, Table 4), while it is practically absent on the methylene groups of **3**$^+$ and quite low on the methylene groups of the rhodium cation radicals [1a]. As already pointed out in Section 2.4, we are inclined to suggest that the conformation of **3**$^+$ (Scheme 3) makes the d-electrons of the metal centres in π symmetry to overlap with the π-orbitals of the bridging fragment and they are delocalized across the connecting ligand and between the two metal centres. In the case of **4**$^+$, hyperconjugation, that results from the interaction of the electrons in methylene σ-bonds with the adjacent π-orbitals, seems to play an important role to give rise to an extended molecular orbital, by virtue of which the odd electron delocalizes over the whole metal–bridge–metal system. It is interesting to underline that, the ancillary ligands being equal, the bimetallic cation radicals **3**$^+$ and **4**$^+$ and the monometallic ones, i.e. **5**$^+$ and **6**$^+$, have, on the base of DFT calculation, the same conformation at the energy minimum, as shown in Fig. 6. Although it is not obvious to understand why do ethylene and carbon monoxide influence the geometry of such species, once again the study points out that a marked role can be indeed played also by the ancillary ligands to the metal in determining the properties of the present class of cyclopentadienyl derivatives, as already noted in the introduction. Finally, we would underline again that 9,10-bis(methylene)anthracene appears an inter-

esting bridging ligand since it, owing to its electronic and conformational properties, can make a strong electronic communication to occur between the linked sites through different ways.

## 4. Experimental details

### 4.1. General procedures

The reactions and manipulations of organometallics were carried out under dinitrogen or argon using standard techniques. All solvents were dried and distilled prior to use following standard procedures. Microanalyses were performed by the Laboratorio di Microanalisi of the Dipartimento di Chimica Bioorganica e Biofarmacia (University of Pisa). $^1$H NMR spectra were run at 200 MHz on a Varian Gemini 200 instrument. Infrared spectra were obtained by a FT-IR Perkin–Elmer 1750 spectrometer. The mass spectrum of **4** was obtained by particle beam-mass spectrometry (PBMS) [8] using a Hewlett–Packard model 5989A mass spectrometer provided with a Hewlett–Packard model 59980A particle beam interface. The flow-injection (FIA) mode was used for sample introduction. Dichloromethane solutions of the complex was injected using a Hewlett–Packard model 1090 HPLC pump; acetonitrile was used as the eluant at a flow-rate of 0.4 ml min$^{-1}$. The nebulizing gas for particle beam interface was high purity helium (inlet pressure 40 psi). The temperature of the desolvation chamber was 40 °C. The mass spectrometer was equipped with a dual electron impact/chemical ionization (EI/CI) source, a hyperbolic mass analyzer, a continuous dinode electron multiplier detector and a differentially pumped vacuum system with diffusion pumps. The Hewlett–Packard MS 59940 ChemStation (HP-UX series) was used as analytical workstation. EI technique was used. The source and the quadrupole temperatures were maintained at 250 and 100 °C, respectively; the ionization energy was 70 eV in the EI mode. The voltage applied to the electron multiplier was 2300 V; the system was scanned from 80 to 800 amu at a rate of 1.16 s per scan. The mass spectra of complexes **3** and **5** were obtained with the Applied Biosystems/MDS Sciex API 4000 triple quadruple mass spectrometry coupled with the Perkin–Elmer Series 200 Micro Pump. Dichloromethane solution of the complex was ionized by Turbo-V Ionspary technique, a variation of ESI-MS. Ionization was performed applying the voltage of 5 kV, and the *declustering* process was carried out using the potential of 20 V.

9,10-Bis[(cyclopentadienylmethyl)thallium(I)]anthracene [1a], chlorodicarbonyl(pyridine)iridium(I) [6], di-μ-chlorotetrakis($\eta^2$-cyclooctene)diiridium(I) [23], ($\eta^5$-cyclopentadienyl)dicarbonyliridium(I) [6], 9-anthrylmethylcyclopentadienylthallium(I) [9] were prepared as reported. 9-Methyl-anthracene (Aldrich), cyclopentadienylthallium(I) (Aldrich), ethylene (Matheson Gas Products), carbon monoxide (Matheson Gas Products), 1,1,1,3,3,3-hexafluoropropan-2-ol (99.8% Aldrich), thallium(III) trifluoroacetate (TTFA) (Aldrich) and [bis(trifluoroacetoxy)iodo]benzene (PIFA) (97% Aldrich) were used as received. *[Owing to their toxicity, all thallium derivatives must be handled with care]*. Tetrabutylammonium hexafluorophosphate (TBAH, puriss. from Fluka) was used as supporting electrolyte as received. Tetrahydrofuran (THF, LiChrosolv, Merck) was treated according to a procedure described elsewhere [24]. For the electrochemical experiments, the solvents were distilled into the electrochemical cell, prior to use, using a trap-to-trap procedure.

### 4.2. UV–Vis absorption and fluorescence emission spectroscopy

The UV–Vis absorption spectra (290–490 nm) were measured at room temperature in dinitrogen-saturated benzene solutions using a Perkin–Elmer UV/VIS LAMDA EZ 201 spectrophotometer with a resolution of 2 nm. The fluorescence spectra (300–600 nm) were measured on an Fluoromax II fluorimeter using an entrance slit width of 1 mm and an exit slit width of 1, 2 or 6 mm depending on the fluorescence emission intensity, spectral resolution is 2 nm. The emission spectra were not corrected for the instrumental response. The relative values of the fluorescence emission intensity were obtained by using the ratio between integral of the emission spectra of compounds and of 9-methylanthracene multiplied 100. All data have been normalized to the same absorbance at the excitation wavelength. Fluorescence emission spectra were registered on benzene solutions under dinitrogen atmosphere. Samples were excited at 333, 343, 353, 363, 373 and 383 nm, emission spectra were collected in the range: excitation wavelengths (+5 nm) to 700 nm.

### 4.3. Electrochemical instrumentation and measurements

The one-compartment electrochemical cell was of air-tight design with high-vacuum glass stopcocks fitted with either Teflon or Kalrez (DuPont) O-rings in order to prevent contamination by grease. The connections to the high-vacuum line and to the Schlenck containing the solvent were obtained by spherical joints also fitted with Viton O-rings. The pressure in the electrochemical cell, prior to performing the trap-to-trap distillation of the solvent, ranged typically from 1.0 to $2.0 \times 10^{-5}$ mbar. The working electrode consisted of a platinum disk microelectrode ($r = 125$ μm) sealed in glass. The counter electrode consisted of a platinum spiral, and the quasi-reference electrode was a silver spiral. The quasi-reference electrode drift was negligible for the time required by a single experiment. Both the counter and the reference electrode were separated from the working electrode by ~0.5 cm. Potentials were measured with the ferrocene standard and are always referred to saturated calomel electrode (SCE). $E_{1/2}$ values correspond to $(E_{pc} + E_{pa})/2$ from CV. For irreversible peaks, the peak potential, $E_p$, is given. Ferrocene was also used as an internal standard for checking the

electrochemical reversibility of a redox couple. Voltammograms were recorded with an AMEL Model 552 potentiostat or a custom-made fast potentiostat controlled by either an AMEL Model 568 function generator or an ELCHEMA Model FG-206F. Data acquisition was performed by a Nicolet Model 3091 digital oscilloscope interfaced to a PC. Temperature control was accomplished within 0.1 °C with a Lauda RL6 thermostat. The minimization of ohmic drop was achieved through the positive feedback circuit implemented in the potentiostat. The DigiSim 3.0 software (Bioanalytical Systems Inc.) was used for digital simulation of CV curves.

### 4.4. EPR experiments

The X-band EPR spectra were obtained by a Varian E112 spectrometer controlling the temperature by an OXFORD EPR 900 cryostat. The EPR spectrometer was interfaced to an IPC 610/P566C industrial grade Advantech computer by means of a data-acquisition system consisting of an acquisition board capable of acquiring up to 500 000 12-bit samples per second including 32-bit add to memory, thus giving on-line signal averaging [25], and a software package specially designed for EPR experiments [26]. The EPR spectra were run by placing the sample (typically 15–20 μL) into quartz tubes (external diameter, 3 mm; internal diameter, 2 mm) fitted with a quartz-Pyrex joint and a Bibby Quickfit Rotaflo PTFE tap (Disa, Milan), according to already published procedures [1,5]. All the EPR experiments were run in a 1:1 (v/v) 1,1,1,3,3,3-hexafluoropropan-2-ol/$CH_2Cl_2$ mixture. Both solvents were saturated with argon before use.

### 4.5. Synthesis of 9,10-bis[($\eta^5$-cyclopentadienylmethyl)-bis($\eta^2$-ethylene)iridium(I)]anthracene (**3**)

Gaseous ethylene is bubbled, for 2.5 h, into an orange solution of di-μ-chlorotetrakis($\eta^2$-cyclooctene)diiridium(I) (0.20 g, 0.22 mmol) in 40 ml of anhydrous tetrahydrofuran, at 0 °C. To the resulting yellow solution of chlorotetrakis($\eta^2$-ethylene)iridium(I)9,10-bis[(cyclopentadienylmethyl)-thallium(I)]anthracene (0.17 g, 0.23 mmol) is added. Immediately, the color of the mixture turns orange-red. The mixture is stirred at room temperature, under ethylene atmosphere, for further 17 h and then filtered. The resulting dark red solution is dried under reduced pressure. The residue is dissolved in 2 ml of benzene and purified by column (internal diameter, 10 mm; length, 300 mm) chromatography on silica gel 60 (230-400 mesh, Merck), using benzene as the eluant, under dinitrogen atmosphere. From the first yellow band eluted, 0.018 g of **3** (0.02 mmol, 9%, yield) are obtained as a yellow microcrystalline powder. Anal. Calc. for $C_{34}H_{36}Ir_2$: C, 49.14; H, 4.37. Found: C, 49.18; H, 4.39%. Turbo-V Ionspray-MS, *m/z*: 831 $[M+H]^+$ ($^{193}$Ir, $^{193}$Ir); 829 $[M+H]^+$ ($^{193}$Ir,$^{191}$Ir); 827 $[M+H]^+$ ($^{191}$Ir,$^{191}$Ir); 775 $[M+H-2C_2H_4]^+$ ($^{193}$Ir, $^{193}$Ir); 773 $[M+H-2C_2H_4]^+$ ($^{193}$Ir, $^{191}$Ir); 747 $[M+H-3C_2H_4]^+$ ($^{193}$Ir, $^{193}$Ir); 745 $[M+H-3C_2H_4]^+$ ($^{193}$Ir, $^{191}$Ir); 743 $[M+H-3C_2H_4]^+$ ($^{191}$Ir, $^{191}$Ir); 725 $[M+H-CH_2C_5H_4-C_2H_4]^+$ ($^{193}$Ir, $^{193}$Ir), 723 $[M+H-CH_2-C_5H_4-C_2H_4]^+$ ($^{193}$Ir, $^{191}$Ir), 721 $[M+H-CH_2C_5H_4-C_2H_4]^+$ ($^{191}$Ir,$^{191}$Ir).

### 4.6. Synthesis of 9,10-bis[($\eta^5$-cyclopentadienylmethyl)-dicarbonyliridium(I)]anthracene (**4**)

A mixture of 9,10-bis[(cyclopentadienylmethyl)thallium(I)]anthracene (0.44 g, 0.6 mmol), chlorodicarbonyl(pyridine)iridium(I) (0.44 g, 1.2 mmol), and benzene (38 ml) is stirred for 24 h, at room temperature and then filtered. The resulting solution is dried under reduced pressure. The residue is dissolved in 2 ml of benzene and purified by column (internal diameter, 10 mm; length, 300 mm) chromatography on alumina (Aluminum oxide 90, 63-200 mesh, Merck), using a 7:3 (v/v) benzene/*n*-hexane mixture as the eluant, under dinitrogen atmosphere. From the second band which elutes 0.15 g of the title compound (0.18 mmol; 31%, yield) are obtained as a pale-yellow microcrystalline powder. Anal. Calc. for $C_{30}H_{20}O_4Ir_2$: C, 43.47; H, 2.42. Found: C, 43.41; H, 2.25%. ESI-MS, *m/z*: 830 $[M]^+$ ($^{193}$Ir, $^{193}$Ir); 828 $[M]^+$ ($^{193}$Ir,$^{191}$Ir); 826 $[M+H]^+$ ($^{191}$Ir, $^{191}$Ir); 802 $[M-CO]^+$ ($^{193}$Ir, $^{193}$Ir); 800 $[M-CO]^+$ ($^{193}$Ir, $^{191}$Ir); 798 $[M-CO]^+$ ($^{191}$Ir, $^{191}$Ir); 774 $[M-2CO]^+$ ($^{193}$Ir,$^{193}$Ir); 772 $[M-2CO]^+$ ($^{193}$Ir,$^{191}$Ir); 770 $[M-2CO]^+$ ($^{191}$Ir,$^{191}$Ir); 746 $[M-3CO]^+$ ($^{193}$Ir, $^{193}$Ir); 744 $[M-3CO]^+$ ($^{193}$Ir, $^{191}$Ir); 742 $[M-3CO]^+$ ($^{191}$Ir, $^{191}$Ir); 718 $[M-4CO]^+$ ($^{193}$Ir, $^{193}$Ir); 716 $[M-4CO]^+$ ($^{193}$Ir, $^{191}$Ir); 714 $[M-4CO]^+$ ($^{191}$Ir, $^{191}$Ir); 554; 525; 360; 332; 183; 113. IR ($C_6H_6$): 3010(s), 2956(s), 2818(s), 2027(s), 1959(s), 1618(s), 1479(s), 1394(s) $cm^{-1}$.

### 4.7. Synthesis of ($\eta^5$-9-anthrylmethylcyclopentadienyl)-bis($\eta^2$-ethylene)iridium(I) (**5**)

Gaseous ethylene is bubbled, for 2.5 h, into an orange solution of di-μ-chlorotetrakis($\eta^2$-cyclooctene)diiridium(I) (0.10 g, 0.11 mmol) in 40 ml of anhydrous tetrahydrofuran, at 0 °C. To the resulting yellow solution of chlorotetrakis($\eta^2$-ethylene)iridium(I), $\eta^5$-9-anthrylmethylcyclo-pentadienylthallium(I) (0.10 g, 0.22 mmol) is added. The resulting mixture is stirred at room temperature, under ethylene atmosphere, for further 18 h and then filtered. The resulting dark red solution is dried under reduced pressure. The residue is dissolved in 2 ml of benzene and purified by column (internal diameter, 10 mm; length, 300 mm) chromatography on silica gel 60 (230-400 mesh, Merck), using 1/1 (v/v) benzene/*n*-hexane mixture as the eluant, under dinitrogen atmosphere. From the first yellow band eluted, 0.03 g of **5** (0.06 mmol, 27%, yield) are obtained as a yellow microcrystalline powder. Anal. Calc. for $C_{24}H_{23}Ir$: C, 57.23; H, 4.60. Found: C, 57.20; H, 4.58%. Turbo-V Ionspray-MS, *m/z*: 505 $[M+H]^+$ ($^{193}$Ir); 503 $[M+H]^+$ ($^{191}$Ir); 527 $[M+Na]^+$ ($^{193}$Ir); 525 $[M+Na]^+$ ($^{191}$Ir); 543 $[M+K]^+$ ($^{193}$Ir); 541 $[M+K]^+$ ($^{191}$Ir); 477 $[M+H-C_2H_4]^+$ ($^{193}$Ir);

449 $[M+H-2C_2H_4]^+$ ($^{193}Ir$); 447 $[M+H-2C_2H_4]^+$ ($^{191}Ir$). $^1H$ NMR ($C_6D_6$), $\delta$ (ppm); 8.30–8.26 (2H, d, $J_{HH}$ 8 Hz, anthrylenic protons); 8.14 (1H, s anthrylenic proton); 7.83–7.79 (2H, d, $J_{HH}$ 8 Hz, anthrylenic protons); 7.33–7.14 (4H, m, anthrylenic protons); 4.58 (2H, d, $J_{HH}$ 1 Hz, $\eta^5$-$C_5H_4$); 4.48 (2H, d, $J_{HH}$ 1 Hz, $\eta^5$-$C_5H_4$); 4.37 (2H, s, $CH_2$); 2.53–2.49 (4H, m, $C_2H_4$); 0.86–0.81 (4H, m, $C_2H_4$).

### 4.8. Synthesis of ($\eta^5$-cyclopentadienyl)bis($\eta^2$-ethylene)-iridium(I) (7)

Compound **7** is obtained by a modified method based on that described [27]. Gaseous ethylene is bubbled, for 2.5 h, into an orange-red solution of di-μ-chlorotetrakis($\eta^2$-cyclooctene)diiridium(I) (0.11 g, 0.12 mmol) in 50 ml of anhydrous diethyl ether, at 0 °C. To the resulting colorless solution of chlorotetrakis($\eta^2$-ethylene)iridium(I), cyclopentadienylthallium(I) (0.07 g, 0.20 mmol) is added at once. Immediately, the color of the mixture turns orange-red. The resulting mixture is stirred at room temperature, under ethylene atmosphere, for 1 h. Afterwards, some decolorizing vegetal charcoal is added to the mixture, which is stirred for a few minutes and filtered. The filtrate is dried under reduced pressure, dissolved in diethyl ether and purified by column (internal diameter, 10 mm; length, 50 mm) chromatography on alumina (Aluminum oxide 90, 70-230 mesh, Merck), using diethyl ether as the eluant, under dinitrogen atmosphere. The first colorless band eluted is collected and dried at reduced pressure. **7** (0.07 g, 0.22 mmol; 92%, yield) is so obtained as a colorless microcrystalline powder. Anal. Calc. for $C_9H_{13}Ir$: C, 34.49; H, 4.18. Found: C, 34.51; H, 4.20%. $^1H$ NMR ($C_6D_6$), $\delta$ (ppm); 4.72 (5H, s, $\eta^5$-$C_5H_5$), 2.72–2.67 (4H, m, $C_2H_4$), 0.82–0.77 (4H, m, $C_2H_4$).

### 4.9. X-ray diffraction studies

Single crystals of **5**, suitable for X-ray analysis, were obtained by cooling a benzene/pentane solution of such a compound. The diffractometric measurements were carried out by using a Bruker-AXS P4 diffractometer equipped with graphite-monochromated Mo Kα radiation. All data were collected in the $\omega/2\theta$ scan mode, and three standard reflections were monitored every 97 measurements to check for possible crystal decay and equipment stability. Data reduction was done through the XSCANS program [28]. A suitable crystal of dimensions $0.44 \times 0.38 \times 0.30$ mm$^3$ was glued at the end of a glass fiber and the unit cell parameters listed in Table 6 were calculated from the setting angles of 38 strong reflections. A set of 4522 intensity data was collected between $1.6° \leqslant \theta \leqslant 25.5°$ and corrected for Lorentz polarization, and absorption effects ($\psi$-scan method). After merging equivalent reflections ($R_{int} = [\sum |F_o^2 - F_o^2(\text{mean})|/\sum(F_o^2)] = 0.0492$), 3665 independent reflections were obtained. The systematic absences pointed to the $P2_1$ or the $P2_1/m$ as possible space groups and the intensity statistics suggested the lack of a centre of symmetry. Thus, the solution was tried in the $P2_1$ space group. The asymmetric unit resulted to be made by two independent molecules approximately related by an inversion centre. This pseudo-centre, however, lies in a position with different $x$ and $z$ coordinates with respect to the screw axis, which are the only true symmetry operators valid for the whole structure. The hydrogen atoms were in part found in the difference Fourier map and in part located in calculated positions; in the last refinement cycles, anisotropic thermal parameters were used for non-hydrogen atoms. The final reliability factors are listed in Table 6. The calculations were done by using the SHELXTL program [29] and some routines contained in the WINGX suite [30]. Possibly due to the presence of some degree of disorder and, maybe, to an incomplete absorption correction, the thermal ellipsoids of some atoms assumed unreliable shapes, in the final stage of refinement, and two rather high residual electron density maxima, i.e. 2.99 and 2.77 e Å$^{-3}$, remained around the iridium atom, at 1.43 and 1.50 Å apart, respectively.

Table 6
Crystal data for **5**

| | |
|---|---|
| Formula | $C_{24}H_{23}Ir$ |
| Formula weight | 503.62 |
| $T$ (K) | 293(2) |
| $\lambda$ (Å) | 0.71073 |
| Crystal system | Monoclinic |
| Space group | $P2_1$ |
| $a$ (Å) | 7.634(8) |
| $b$ (Å) | 24.358(10) |
| $c$ (Å) | 10.117(4) |
| $\beta$ (°) | 103.46(3) |
| $V$ (Å$^3$) | 1830(2) |
| $Z$ | 4 |
| $D_{calc}$ (g cm$^{-3}$) | 1.828 |
| $\mu$ (Mo Kα) (mm$^{-1}$) | 7.298 |
| $F$(000) | 976 |
| Reflections collected | 4522 |
| Independent reflections ($R_{int}$) | 3665 (0.0492) |
| Parameters | 425 |
| Goodness-of-fit on $F^2$ | 1.014 |
| Final $R$ indices [$I > 2\sigma(I)$] | $R_1 = 0.0503$, $wR_2 = 0.1092$ |
| $R$ indices (all data) | $R_1 = 0.0909$, $wR_2 = 0.1280$ |

## Acknowledgments

We are grateful to Dr. A. Raffaelli and Dr. A. Saba (C.N.R., Pisa, Italy) for the measurement of the ESI MS mass spectra, to Prof. M. Careri (University of Parma, Italy) for the measurement of the PBMS mass spectra, and to Professor M. Zandomeneghi for the measurement of fluorescence spectra. Financial supports from the M.I.U.R. (Rome, Italy) (PRIN and FIRB), from the University of Pisa, and from the University of Bologna (Funds for Selected Research Topics) are gratefully acknowledged.

## Appendix A. Supporting information

X-ray crystallographic data (CIF file) for the structure of **5**, which has been deposited with the Cambridge

Crystallographic Data Centre with reference number CCDC 274745, is also available free of charge via the Internet at http://www.pubs.acs.org. Supplementary data associated with this article can be found, in the online version, at doi:10.1016/j.jorganchem.2006.03.017.

## References


[1] (a) M. Carano, M. Careri, F. Cicogna, I. D'Ambra, J.L. Houben, G. Ingrosso, M. Marcaccio, F. Paolucci, C. Pinzino, S. Roffia, Organometallics 20 (2001) 3478;
(b) F. Cicogna, B. Gaddi, G. Ingrosso, M. Marcaccio, F. Marchetti, D. Paolucci, F. Paolucci, C. Pinzino, R. Viglione, Inorg. Chim. Acta 357 (2004) 2915.

[2] (a) V. Balzani, F. Scandola, Supramolecular Photochemistry, Ellis Horwood, New York, 1991;
(b) R.A. Bissel, A.P. De Silva, H.Q.N. Gunaratne, P.L. Lynch, G.E. Maguire, C.P. McCoy, K.R.A.S. Sandanayake, Top. Curr. Chem. 168 (1993) 223;
(c) F. Paul, C. Lapinte, Coord. Chem. Rev. 178–180 (1998) 431;
(d) L. De Cola, P. Belser, Coord. Chem. Rev. 177 (1998) 301;
(e) R. Ziessel, M. Hissler, A. El-ghayoury, A. Harriman, Coord. Chem. Rev. 178–180 (1998) 1251;
(f) P.F. Pina, M.A. Bernardo, E. García-España, Eur. J. Inorg. Chem. (2000) 2143;
(g) N. Di Cesare, J.R. Lakowicz, Anal. Biochem. 294 (2001) 154;
(h) C.G. De Azevedo, K.P.C. Vollhardt, Synlett (2002) 1019;
(i) Y.S. Han, S.D. Kim, L.S. Park, D.U. Kim, Y.H. Kwon, J. Polym. Sci. A 41 (2003) 2502;
(j) F.B. Xu, Q.S. Li, X.S. Zeng, X.B. Leng, Z.Z. Zhang, Organometallics 23 (2004) 632;
(k) A. Ceccon, S. Santi, L. Orian, A. Bisello, Coord. Chem. Rev. 248 (2004) 683;
(l) S.K. Kim, N.J. Singh, S.J. Kim, K.M.K. Swamy, S.H. Kim, K.H. Lee, K.S. Kim, J. Yoon, Tetrahedron 61 (2005) 4545.

[3] M.B. Robin, P. Day, Adv. Inorg. Chem. Radiochem. 10 (1967) 247.

[4] V. Balzani, A. Juris, M. Venturi, S. Campagna, S. Serroni, Chem. Rev. 96 (1996) 759.

[5] M. Carano, F. Cicogna, I. D'Ambra, B. Gaddi, G. Ingrosso, M. Marcaccio, D. Paolucci, F. Paolucci, C. Pinzino, S. Roffia, Organometallics 21 (2002) 5583.

[6] M.S. Blais, M.D. Rausch, J. Organomet. Chem. 502 (1995) 1.

[7] J.W. Kang, K. Moseley, P.M. Maitlis, J. Am. Chem. Soc. 91 (1969) 5970.

[8] (a) M. Careri, A. Mangia, P. Manini, G. Predieri, E. Sappa, J. Organomet. Chem. 476 (1994) 127;
(b) M. Careri, A. Mangia, P. Manini, G. Predieri, E. Licandro, A. Papagni, Rapid Commun. Mass Spectrom. 11 (1997) 51;
(c) M. Careri, C. Graiff, A. Mangia, P. Manini, G. Predieri, Rapid Commun. Mass Spectrom. 12 (1998) 225.

[9] F. Cicogna, M. Colonna, J.L. Houben, G. Ingrosso, F. Marchetti, J. Organomet. Chem. 593–594 (2000) 251.

[10] S.N. Paisner, G.G. Lavoie, R.G. Bergman, Inorg. Chim. Acta 334 (2002) 253.

[11] R.N. Jones, J. Am. Chem. Soc. 67 (1945) 2127.

[12] H.H. Jaffé, M. Orchin, Theory and Applications of Ultraviolet Spectroscopy, Wiley, New York, 1962.

[13] (a) A.J. Bard, L.R. Faulkner, Electrochemical Methods: Fundamentals and Applications, Wiley, New York, 2001, pp. 200–201 (Chapter 12);
(b) C. Bruno, I. Doubitski, M. Marcaccio, F. Paolucci, D. Paolucci, A. Zaopo, J. Am. Chem. Soc. 125 (2003) 15738;
(c) N. Camire, A. Nafady, W.E. Geiger, J. Am. Chem. Soc. 124 (2002) 7260.

[14] M. Krejčik, A.A. Vlček, J. Electroanal. Chem. 313 (1991) 243.

[15] S. Campidelli, E. Vazquez, D. Milic, M. Prato, J. Barbera, D.M. Guldi, M. Marcaccio, D. Paolucci, F. Paolucci, R. Deschenaux, J. Mater. Chem. 14 (2004) 1266, and references therein.

[16] Spartan'02, Wavefunction, Inc. 18401 Von Barman Avenue, Suite 370 Irvine, CA 92612, USA.

[17] A.D. Becke, J. Chem. Phys. 98 (1993) 5648.

[18] C. Lee, W. Yang, R.G. Parr, Phys. Rev. (1988) 785.

[19] (a) A. Fortunelli, O. Salvetti, J. Mol. Struct. (Theochem) 287 (1993) 89;
(b) A. Fortunelli, Int. J. Quantum Chem. 52 (1994) 97.

[20] J.A. Degray, P.H. Rieger, N.G. Connelly, G. Garcia Herbosa, J. Magn. Reson. 88 (1990) 376.

[21] S. Berger, A. Klein, M. Wanner, W. Kaim, J. Fiedler, Inorg. Chem. 39 (2000) 2516.

[22] J.A. Pople, D.L. Beveridge, Approximate Molecular Orbital Theory, McGraw-Hill, New York, 1970.

[23] A.L. Onderdeliden, A. Van der Ent, Inorg. Chim. Acta 6 (1972) 420.

[24] M. Carano, P. Ceroni, L. Mottier, F. Paolucci, S. Roffia, J. Electrochem. Soc. 146 (1999) 3357.

[25] R. Ambrosetti, D. Ricci, Rev. Sci. Instrum. 62 (1991) 2281.

[26] C. Pinzino, C. Forte, EPR-ENDOR, ICQEM-CNR Rome, Italy, 1992.

[27] (a) J.M. Mayer, J.C. Calabrese, Organometallics 3 (1984) 1292;
(b) T.W. Bell, D.M. Haddleton, A. McCamley, M.G. Partridge, R.N. Perutz, H. Willner, J. Am. Chem. Soc. 112 (1990) 9212;
(c) D.M. Heinekey, J.M. Millar, T.F. Koetzle, N.G. Payne, K.W. Zilm, J. Am. Chem. Soc. 112 (1990) 909;
(d) L.P. Szajek, R.J. Lawson, J.R. Shapley, Organometallics 10 (1991) 357.

[28] XSCANS, X-ray Single Crystal Analysis System, Rel.2.1, Bruker AXS Inc., Madison, WI, USA, 1994.

[29] G.M. Sheldrick, SHELXTL-PLUS, Rel.5.1, Bruker AXS Inc., Madison, WI, USA, 1997.

[30] L.J. Farrugia, J. Appl. Crystallogr. 32 (1999) 837.